New advances in magnetic nanostructures

J.L. Morán-López
División de Materiales Avanzados para la Tecnología Moderna,
Instituto Potosino de Investigación Científica y Tecnológica,
San Luis Potosí, S.L.P., México.

Recibido el 9 de junio de 2006; aceptado el 6 de noviembre de 2006

Some of the new developments on magnetic nanostructures are reviewed. The advances on the synthesis, characterization, and understanding of magnetic nanoclusters, magnetic nanowires and single molecule magnets are discussed. Particular emphasis is made on the magnetic properties of: a) magnetic iron nanowires encapsulated in carbon nanotubes, and b) manganese nanostructures which show a very rich and complex behavior. Both systems are good candidates for technological applications.

Keywords: Magnetic nanostructures; nanowires; iron nanostructures; manganese nanostructures.

Se discuten algunos de los avances recientes en materiales magnéticos nanoestructurados. Se analizan los avances recientes en la síntesis, caracterización, y entendimiento de las propiedades magnéticas de agregados atómicos, nanoalambres y magnetos de una sola molécula. En particular se hace énfasis en las propiedades magnéticas de: a) nanoalambres magnéticos de hierro encapsulados en nanotubos de carbón y b) en nanoestructuras de manganeso, las cuales muestran una gran riqueza de comportamiento magnético. Ambos sistemas tienen buenas posibilidades de aplicaciones tecnológicas.

Descriptores: Nanoestructuras magnéticas; nanoalambres; nanoestructuras de hierro; nanoestructuras de manganeso.

PACS: 81.07.Dc; 75.75.+a; 36.40.Cg

1. Introduction

Due to the effects of special confinement and low dimensionality, ultra thin films, nanowires, and clusters of atoms composed of transition metal atoms exhibit magnetic properties not displayed by the corresponding bulk solids. For example, elements that do not show magnetic phases in bulk, like rhodium, display magnetic moments in small clusters [1]. Furthermore, due to recent advances in experimental techniques, nowadays one can synthesize, characterize and design special materials with specific size, composition and structure. It is interesting that these new materials show unexpected physicochemical properties that are not interpolations between the atomic or molecular structures and the bulk solids. These effects are recognized to be produced mainly by the large ratio between surface and bulk atoms [2].

In particular, the magnetic properties of low dimensional systems are of great importance from both, the point of view of fundamental understanding, and for the potential applications in storage media. Careful measurements of the magnetic properties of small magnetic aggregates, nanowire arrays and single molecule magnets have been published in the last decade. In the case of small atomic clusters, most of them show an enhancement in the atomic magnetic moments and a smooth size dependence [3]. An exemption is manganese, which by far is the most complicated magnetic element. The size dependence of the magnetic moment is non monotonic with various maxima [4].

On the other hand, other systems that exhibit potential technological applications are nanowires of transition metals. It has been reported two ways to synthesize them. One is to fill carbon nanotubes with magnetic materials [5] and the other is to fill nanopourous templates with a well defined geometry [6].

Here, I report results on two particular systems. First I will mention results on the magnetic behavior of carbon nanotubes filled with iron [7] and then I will report on recent results on the magnetic properties of manganese clusters [8]. Details on the two subjects can be found in the given references.

2. Carbon nanotubes filled with Fe

Carbon nanotubes can be considered as rigid cylindrical nano-containers able to host gaseous molecules and solids [9]. By means of thermolytic routes involving the carbon decomposition of organic precursors over transition metals such as Fe, Co and Ni, it has been produced nanotubes filled with these ferromagnetic materials [10]. The method has also been able to generate arrays of aligned nanotubes filled with pure ferromagnetic crystalline nanowires, oriented along a preferred crystalline direction. In addition, the carbon coating the wire prevents the oxidation of the wire, thus avoiding anti-ferromagnetic contributions in the systems. These arrays of Fe wires inside carbon nanotubes (FeNWs@MWNTs), exhibiting magnetic coercivities 10–30 times larger than bulk Fe, could be used as high density magnetic storage media (*e.g.* > 50 Gbit/in^2) [11].

As mentioned above, efforts in fabricating high density magnetic storage devices using arrays of bare ferromagnetic nanowires (not encapsulated in carbon nanotubes and possibly containing oxide layers) have been reported, and were produced using various methods involving: (a) alumina channel templates [12]; (b) patterned substrates [13], or (c) copolymer techniques [14]. A disadvantage of the lat-

ter techniques is the creation of an oxide layer coating the ferromagnetic nanowire, which generates antiferromagnetic moments that perturb the system and the storage capacity. However one of the best advantages of these arrays is that they can be produced with controlled characteristics and form monodisperse arrangements.

The experimental samples consisted of aligned Fe-filled carbon nanotubes doped with nitrogen (CN_x) produced by pyrolyzing benzylamine: ferrocene mixtures in an Ar atmosphere at 850°C. In the inset of Fig. 1, a scanning electron microscope (SEM) image of aligned Fe filled CN_x nanotubes is shown. The image clearly indicates that the tubes grow perpendicular to the substrate and are highly compacted. The Fe wires consist of single nanocrystals oriented with the Fe(100) plane parallel to the wire axis of the bcc phase, and they are oxygen free as reveled by electron energy loss spectroscopy analysis.

The magnetic susceptibility and magnetization was measured using a Quantum Desing SQUID magnetic property measurement system while the resistivity magnetoresistance was measured by means of a Quantum design physical property measurement system. In order to obtain further understanding of the low temperature behavior of the magnetic susceptibility and the resistivity, we carried out isothermal magnetization and magnetoresistance measurements with an applied magnetic field H parallel and perpendicular to the Fe filled CN_x nanotubes.

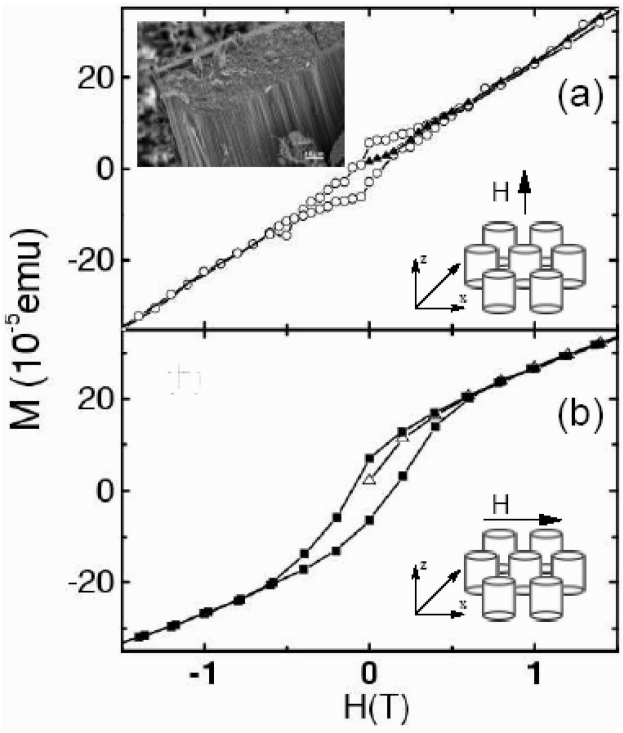

FIGURE 1. Hysteresis loops measured at 1.8 K for a carpet consisting of compacted ferromagnetic Fe nanowires encapsulated in C nanotubes. The magnetic field was applied (a) parallel and (b) perpendicular to the nanowires.

Figure 1 exhibits the hysteresis loop for H applied parallel and perpendicular to filled tubes. Previous results found in nanowires fabricated in alumina material [12], where the dipolar interactions between the nanowires were neglected because the large distance between the cylinders, indicate that the hysteresis loops are narrower for perpendicularly applied magnetic fields. In contrast to these reports, our results show the opposite behavior, that is, our samples display wider hysteresis loops when external fields are applied perpendicular to the wire [see Fig. 1(b)] than when an external field is applied parallel to the wire axis [see Fig. 1(a)]. We attribute this behavior to the dipolar interactions and small aspect ratio within the Fe wires, dominant in our samples due to the close-packing of the Fe filled tubes.

One observes also that the hysteresis loop exhibits clear steps when the magnetic field is applied parallel to the wire axis. That is not the case when the field is applied in a perpendicular direction in which case the hysteresis loop shows a continuous reversal magnetization.

Due to the great degree of freedom of the magnetic moments within Fe wires under the presence of a magnetic field, a well-suited model which could account for it and for its behavior in general is the classical Heisenberg Hamiltonian for localized spins on a lattice.

$$H = -J \sum_{i,j \in nn} \vec{\mu}_i \cdot \vec{\mu}_j - D \sum_{i \neq j} P_{ij} - \sum_{i=1} \vec{H} \cdot \vec{\mu}_i \,, \qquad (1)$$

with

$$P_{ij} = \frac{[\vec{\mu}_i \cdot \vec{\mu}_j - 3(\vec{\mu}_i \cdot \hat{e}_{ij})(\vec{\mu}_j \cdot \hat{e}_{ij})]}{r_{ij}^3} \,, \qquad (2)$$

where $\vec{\mu}_i$ is the three dimensional magnetic moment of unit length in site i and with components given by $(\mu_{i,x}, \mu_{i,y}, \mu_{i,z})$ and i runs between 1 and the total number of atoms n. Observe that this Hamiltonian has been scaled by the spin magnetic moment μ_s, so that $\vec{\mu}_i$ is a unit vector ($\vec{\mu}_i = \vec{\mu}_i/\mu_s$). The first sum represents the ferromagnetic exchange with constant coupling J, this sum only accounts for first neighbors (nn). The second term describes the dipole-dipole interaction and with $D = \mu_0 \mu_s^2/(4\pi a^3)$ describing the strength of the interaction ($\mu_0 = 4\pi \times 10^{-7} Vs/Am$ and a is the lattice parameter). The vector $\hat{e}_{ij}$ is a unit vector pointing from lattice site i to j. The third term refers to the external magnetic field to the energy contribution.

The minimum energy spin configuration has been searched using MC method with the Metropolis algorithm. We start the MC sequence with a random spin configuration, and we stop after 1×10^5 MC steps, where non variation of the energy is observed. For an elementary process a random spin chosen is flipped if the energy decreases and otherwise the In Fig. 2 we show the results for the magnetic behavior of a bundle of nanowires arranged in a hexagonal fashion. Each wire contains 31 atoms and the wire aspect ratio corresponds to $L/d \approx 1.5$. We noted that for interwire distances smaller than 9.4 Å, cohercive fields are always small for fields applied parallel to the wires axes. For fields applied perpen-

dicular to the wires, cohercive field values are enhanced for narrow interwire distances.

When the magnetic field was applied parallel to the wire axis, the reversal magnetization mechanism is characterized by complex magnetic states that are shown in Fig. 2. Starting with a state of complete magnetization (Fig. 2a) we observe in Fig. 2b a canted state configuration that starts to change abruptly due to polar interactions, promoting the creation of helical vortices at positive low external magnetic fields (Fig. 2c). Following slight increments of the magnetic field, a vortex state appears at zero magnetization (Fig. 2d). This vortex state reveals an almost linear behavior of the magnetization from point d to e. Subsequently an abrupt change of the magnetization (from point e to f) is observed and the wire array exhibits another helical spin configuration. Finally for larger magnetic fields the systems saturates following a continuous magnetic behavior (sequence f-g-h-i).

Comparing these results with the experimental observations, one distinguishes strong similarities. For example Fig. 1a depicts abrupt steps at low magnetic fields, which we interpret as arising from the creation of 3D helical vortices.

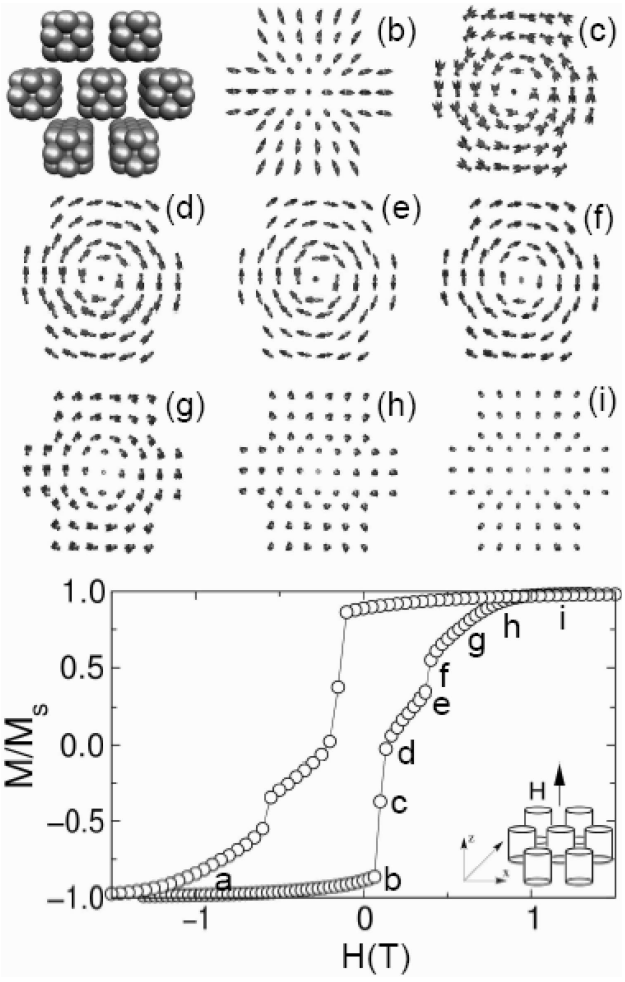

FIGURE 2. Hysteresis loop simulations obtained for an hexagonal array of nanowires with interwire distance of 7.2 Å.

3. Magnetic properties of Mn_n clusters

Manganese is a unique element which exhibits a variety of unusual electronic and magnetic properties depending on the environment. For instance, the bulk-crystal structure of α-Mn is remarkably complex. It contains 29 atoms in the unit cell and shows antiferromagnetic ordering [15]. On the other hand, dilute solutions of Mn in Cu behave like spin glasses [16]. Also, the compounds known as manganites show fascinating magnetic properties [17]. In addition, Mn_{12}-complexes act as molecular magnets, exhibiting resonant tunneling between spin states [18] and forming "nano-domains" [19, 20]. Finally, the manganese dimer is Van der Waals bonded and also seems to exhibit antiferromagnetic behavior [21].

Consistently with the remarkable properties of Mn-compounds mentioned above, and despite the similar magnetic ordering of Mn_2 and Mn-bulk, experiments show that small manganese clusters exhibit an intriguing magnetic behavior, with signatures of super paramagnetism and magnetic moments $\mu(n)$ smaller than $1.5\mu_B$ per atom [4], furthermore, the behavior of $\mu(n)$ as a function of n is strongly non monotonous.

In the last years, different theoretical determinations of the magnetic and electronic structure of Mn_n clusters have been reported [8]. Almost all calculations have in common the assumption of collinear spins, but give contradictory results.

The experimental evidence and the theoretical works mentioned above suggest that the most probable scenario for small Mn clusters is that of almost degenerate different spin configurations. Therefore, the correct approach to describe their magnetic structure must give up the assumption of collinearity. This was confirmed recently by a calculation which yields a noncollinear magnetic configuration for Mn_6 [22]. Moreover, the fact that the ferromagnetic and antiferromagnetic solutions are very close in energy, in particular for very small clusters leads also to spin frustration in larger clusters.

Here, we present the first theoretical description of the size dependence $\mu(n)$ for Mn_n clusters up to $n = 40$, which accounted [8] for most of the experimental findings, reported by Knikelbein [4].

We performed first a noncollinear *ab-initio* determination of the magnetic properties of small Mn_n clusters on the range $2 \leq n \leq 8$. Our results suggest that in small Mn_n clusters a remarkable competition between kinetic and exchange-correlation energies leads to almost degenerate spin configurations which result in the formation of noncollinear magnetic nano-domains in order to avoid spin frustration. Moreover, with the help of the data obtained from the *ab-initio* calculations we fit the parameters of an effective Spin-Hamiltonian, which we used to calculate $\mu(n)$ for larger clusters ($9 \leq n \leq 40$). This model gives very good agreement with the puzzling experimental results.

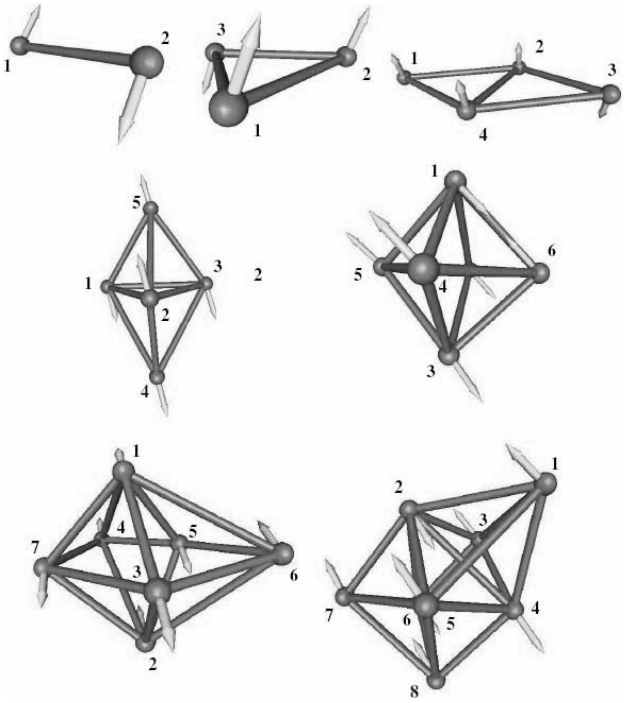

FIGURE 3. Ground-state structures of Mn_n clusters, for $n = 2-8$, optimized with respect to the electronic, ionic and spin degrees of freedom. The magnitude and orientation of the quantum expectation value of the spin at each atom is indicated by arrows.

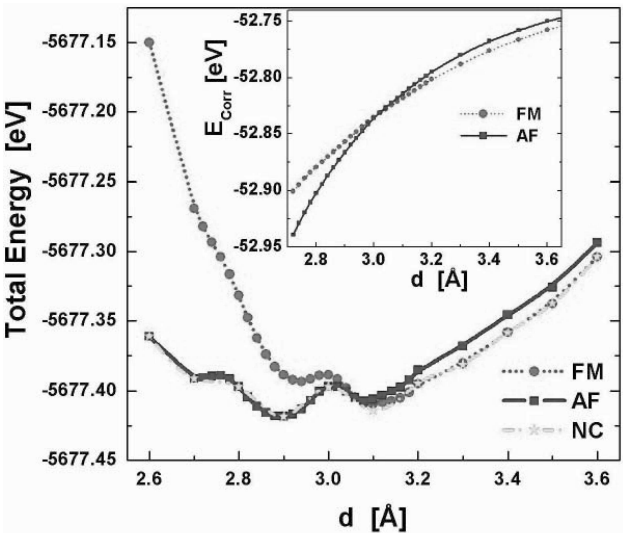

FIGURE 4. Total electronic energy of Mn_2 as a function of the interatomic distance for the noncollinear, ferromagnetic and antiferromagnetic cases. The crossing at $d = 3.06$ Åcan be clearly observed. Inset: distance dependence of the correlation energy for Mn_2 as function of distance for the ferro- and antiferromagnetic configurations. Note that the crossing occurs at the same distance as for the total energies.

To determine the electronic and magnetic properties of the clusters in the range $2 \leq n \leq 8$ we have used the SIESTA code [23], which performs a fully self-consistent density-functional calculation to solve the Kohn-Sham equations. We included spin polarization, both collinear and noncollinear, in the local-density approximation (LDA). Details of the calculation can be found in Ref. 8.

In Fig. 3 we show the ground-state structures and spin configurations obtained from the *ab-initio* calculations. Interestingly, most of these clusters, in particular $n = 6, 7$ and 8, show noncollinear magnetic behavior. This indicates that previous theoretical studies, with the exception of reference [22], missed an essential ingredient for the correct physical description of these systems. As can be seen from Fig. 3, some of the clusters show a marked Jahn-Teller distortion, like Mn_3 and Mn_4. As a general rule, the average magnetic moment μ of these clusters is at least two times smaller than the moment of an isolated Mn atom. The average magnetic moments obtained are: $\mu(2) = 0$, $\mu(3) = 1.67\mu_B$, $\mu(4) = 2.5\mu_B$, $\mu(5) = 1.0\mu_B$, $\mu(6) = 0.87\mu_B$, $\mu(7) = 0.99\mu_B$, and $\mu(8) = 1.17\mu_B$. Note that the lowest energy structure of Mn_5 corresponds to an almost bipyramidal configuration. However, symmetry is broken due to the formation of domains. A similar effect is present for $n = 6, 7$ and 8. Apart from the noncollinear behavior, the most important feature of the magnetic configurations shown in Fig. 3 is that manganese atoms separated by short distances are mostly coupled antiferromagnetically, whereas for long interatomic distances the coupling is mostly ferromagnetic. This remarkable effect leads to spin frustration and the formation of noncollinear nanodomains, as clearly shown in Fig. 3.

In fact, the nature of magnetism in small Mn_n clusters can be inferred from the magnetic behavior in the dimer. Although almost all *ab-initio* studies performed so far for Mn_2 obtained a ferromagnetic configuration, our calculations yield an antiferromagnetic state, with a bond length of $r_0 = 2.890$ Å . This result for the magnetic ordering of the dimer is in agreement with the existing experimental evidences [21]. However, it must be pointed out that the ferromagnetic, antiferromagnetic and noncollinear states are almost degenerate. Interestingly, if we now force the interatomic distance to be equal to the experimental value $r_0^{exp} = 3.18$ Å [24] we obtain a ferromagnetic ground-state. This fact is originated from a remarkable distance dependence exhibited by the magnetic coupling. To analyze this in detail we plot in Fig. 4 the total energy of the dimer as a function of the bond length d for the collinear ferromagnetic and antiferromagnetic configurations and also for the noncollinear solution. The most important feature of Fig. 4 is that there is a crossing between the FM and AF curves at $d_c = 3.06$ Å , which determines the interatomic distance at which the ground-state changes from anti- to ferromagnetic. Note that the energy of the noncollinear solution coincides with the AF curve for distances for $d < d_c$ and with the FM curve for $d > d_c$. This means that the dimer shows collinear magnetism for almost all distances. However, we obtain an interesting behavior around $d = d_c$, where the noncollinear solution has a slightly lower energy than the collinear curves. This is due to the fact that at this point the AF and FM states have the same energy and therefore an intermediate noncollinear state leads to an energy decrease.

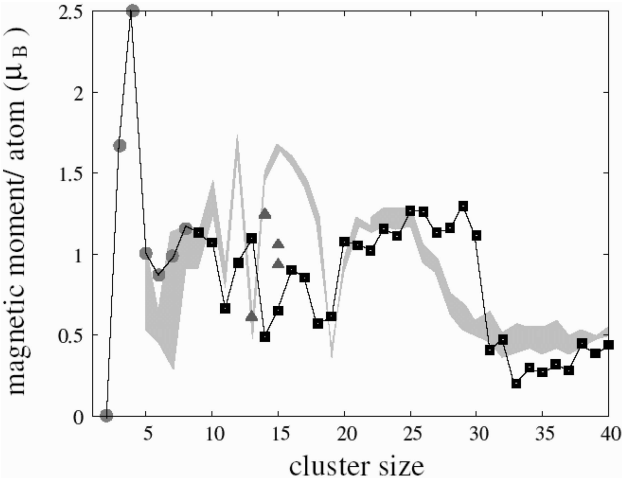

FIGURE 5. Size dependence of the magnetic moment per atom μ (in units of μ_B) of Mn_n clusters in the size range $2 \leq n \leq 40$. Red circles correspond to the *Ab-initio* results. Squares show the calculated μ for compact structures using the classical Spin-Hamiltonian of Eq. (2). Grey Open triangles refer to isomers having smaller cohesive energies. The light-blue shadowed zone corresponds to the experimental results of Ref. 4 taken into account the reported error bars.

We have compared the distance dependence of the different terms contributing to the cohesive energy of the dimer. It turns out that most of the energies cancel each other, so that the correlation energy plays a fundamental role. In the inset of Fig. 4 we show the bond-length dependence of the correlation energy for the ferromagnetic and antiferromagnetic configurations. Notice that for $d < d_c$ the correlation energy favors antiferromagnetic behavior, while for larger distances the correlation energy term of the ferromagnetic state becomes slightly more important. Since the FM and the AF configurations of the dimer are very close in energy, and due to the change of magnetic character for increasing distances, one should not expect a clear magnetic ordering in small clusters, but rather a competition between both types. The fact that nearest neighbors will tend to order antiferromagnetically, whereas further neighbors will favor a ferromagnetic ordering leads to noncollinear effects, domain formation, in order to avoid spin frustration as much as possible.

The behavior shown in Fig. 4 can be interpreted as follows. For short interatomic distances the strong overlap of 3d-orbitals leads to an electron delocalization, which favors antiferromagnetism. In contrast, for long distances, localization becomes more important and ferromagnetic correlations dominate. This explains the calculated spin configurations for Mn_5 to Mn_8 (Fig. 3).

Now, and in order to determine the magnetic properties of clusters with n up to 40, which cannot be done yet using *ab-initio* approaches we propose an effective spin Hamiltonian of the form

$$H = \sum_{\substack{i,j=1,n \\ i \neq j}}^{n} J_{ij}\, \vec{S}_i \cdot \vec{S}_j \; + \; V(\{|\vec{r}_i - \vec{r}_j|\}), \qquad (3)$$

where the $\vec{S}_i$ are classical spins, with magnitudes measured in Bohr magnetons. The exchange coupling constants J_{ij} are the distance dependent quantities $J(|\vec{r}_i - \vec{r}_j|)$, being $|\vec{r}_i - \vec{r}_j|$ the distance between atoms i and j. We use for $J(|\vec{r}_i - \vec{r}_j|)$ the function $J(d)$ extracted from the dimer. Moreover, we analyzed carefully the local magnetic moments S_i obtained from the *ab-initio* calculations (Mn_2 to Mn_8) as a function of the coordination number z, and we obtained a clear relation between them. It turns out that a function of the form $S = 4.42 - 0.5z$ for $z \leq 8$ and $S_i = 0.4$ for $z > 8$, reproduces the results obtained for small clusters. The coordination number z_i of atom i is defined as the number of neighbors being at a distance smaller than 2.26 Å(nearest neighbor distance in bulk-Mn) from atom i. It must be pointed out that, although the spins $\vec{S}_i$ are treated as classical, the scalar product is taken into account. Therefore, the Hamiltonian H intrinsically includes noncollinearity.

In Eq. 2, $V(\{|\vec{r}_i - \vec{r}_j|\})$ is, in general, a many-body potential which models the cohesive energy of the cluster. For simplicity, we take a Lennard-Jones-type (LJ) potential in order to generate compact structures, which are expected for cluster in the size range we are interested in.

We minimized H numerically, by using genetic algorithms, and obtained the ground state spin-configurations for clusters up to Mn_{40}. The calculated size dependence of the magnetic moments per atom is shown in Fig. 5, where we also show the *ab-initio* results. Clearly, the orders of magnitude of the all calculated magnetic moments are in good agreement with experiment. Moreover, the overall size dependence $\mu(n)$ is well described and shows a complex behavior, as in the experiment [4]. Note that in our results the oscillations as a function of n between $n = 6$ and $n = 13$, $n = 14$ and $n = 20$, and between $n = 21$ and $n = 31$, observed in experiment, are very well reproduced.

In Fig. 5 we also show the magnetic moments of isomers of Mn_{13}, Mn_{14} and Mn_{15} which have smaller cohesive energy than the ground-state structures, but which might also be present in the cluster beam on which experiments have been performed. The good agreement between our model and experiment indicates that the physics underlying our model is correct, *i.e.*, the magnetic properties of Mn_n clusters are dominated by spin frustration due to the presence of different spin-spin coupling constants, which leads to noncollinear magnetism and formation of nanodomains. As a consequence, $\mu(n)$ shows a complex form and low magnetic moments, which reflect the least frustrated possible spin configurations.

4. Summary

Summarizing, I presented results on two particular nanomagnetic systems; iron nanowires encapsulated in carbon nanotubes and small manganese clusters. These are examples of the very rich variety of magnetic systems at the nanometer scale. This is a field of very intensive research in which

the applications foreseen are very important. For storage applications it is necessary to have monodisperse systems. Good candidates are nanowires grown in nanoporous templates and one single molecule magnets, discovered recently. Still, many studies are necessary to understand those very interesting nanostructures.

1. A.J. Cox, J.G. Louderback, and L.A. Bloomfield, *Phys. Rev. Lett.* **71** (1993) 923.
2. J.L. Morán-López, *Computational Materials Science* **2** (1994) 72.
3. I.M. Billas, A. Châtelain, and W.A. de Heer, *Science* **265** (1994) 1682.
4. M.B. Knickelbein, *Phys. Rev. B* **70** (2004) 014424.
5. R. Kamalakaran *et al.*, *Appl. Phys. Lett.* **77** (2000) 3385.
6. T. Thurn-Albrecht *et al.*, *Science* **290** (2000) 2126.
7. F. López-Urías *et al.*, *Physical Review Letters* **94** (2005) 216102.
8. J. Mejía-López, A.H. Romero, M.E. García, and J.L. Morán-López, *Phys. Rev. B, Rapid Commun.* **74** (2006) 140405.
9. M. Terrones, *Annu. Rev. Mater. Res.* **33** (2003) 419.
10. C.N.R. Rao, R. Sen, B.C. Satishkumar, and A. Govindaraj, *Chem. Comm.* **15** (1998) 1525.
11. N. Grobert *et al.*, *Appl. Phys. Lett.* **75** (1999) 3363.
12. Y. Peng, H.L. Zhang, S.L. Pan, and H.L. Lee, *J. Appl. Phys.* **87** (2000) 7405.
13. M. Hehn *et al.*, *Science* **272** (1996) 1782.
14. T. Thurn-Albretch *et al.*, *Science* **290** (2000) 2126.
15. D. Hobbs, J. Hafner, and D. Spisak, *Phys. Rev. B* **68** (2003) 014407.
16. D. Chu, G.G. Kenning and R. Orbach, *Phys. Rev. Lett.* **72** (1994) 3270.
17. Elbio Dagotto, in *The Physics of Manganites and Related Compounds* (Springer Series in Solid-State Sciences, 2003) Vol. 136.
18. J.R. Friedman, M.P. Sarachik, J. Tejada, and R. Ziolo, *Phys. Rev. Lett.* **76** (1996) 3830.
19. W. Wensdorfer, N. Aliaga-Alcalde, D. N. Hendrickson, G. Christou, *Nature* **416** (2002) 406.
20. R. Sessoli, D. Gatteschi, A. Caneshi, and M.A. Novak, *Nature* **365** (1993) 141.
21. J.R. Lombardi and B. Davids, *Chem. Rev.* **102** (2002) 2431.
22. T. Morisato, S.N. Khanna, and Y. Kawazoe, *Phys. Rev. B* **72** (2005) 014435.
23. E. Artacho, D. Sánchez-Portal, P. Ordejón, A. García, and J.M. Soler, *Phys. Status Solidi B* 215 (1999) 809.
24. R.J. Van Zee, C.A. Baumann, S.V. Bhat, and W. Weltner, Jr., *J. Chem Phys.* **76** (1982) 5636.